

# Unnatural Peptide Assemblies Rapidly Deplete Cholesterol and Potently Inhibit Cancer Cells

Qiuxin Zhang, Weiyi Tan, Zhiyu Liu, Yichi Zhang, Wei-Shao Wei, Seth Fraden, and Bing Xu\*



Cite This: *J. Am. Chem. Soc.* 2024, 146, 12901–12906



Read Online

ACCESS |



Metrics & More



Article Recommendations



Supporting Information

**ABSTRACT:** Cholesterol-rich membranes play a pivotal role in cancer initiation and progression, necessitating innovative approaches to target these membranes for cancer inhibition. Here we report the first case of unnatural peptide (**1**) assemblies capable of depleting cholesterol and inhibiting cancer cells. Peptide **1** self-assembles into micelles and is rapidly taken up by cancer cells, especially when combined with an acute cholesterol-depleting agent ( $M\beta CD$ ). Click chemistry has confirmed that **1** depletes cell membrane cholesterol. It localizes in membrane-rich organelles, including the endoplasmic reticulum, Golgi apparatus, and lysosomes. Furthermore, **1** potently inhibits malignant cancer cells, working synergistically with cholesterol-lowering agents. Control experiments have confirmed that C-terminal capping and unnatural amino acid residues (i.e., BiP) are essential for both cholesterol depletion and potent cancer cell inhibition. This work highlights unnatural peptide assemblies as a promising platform for targeting the cell membrane in controlling cell fates.

This communication reports an unexpected observation that unnatural peptide assemblies deplete cholesterol in the cell membrane to inhibit cancer cells. Cholesterol is crucial for both membrane integrity and cancer development.<sup>1,2</sup> Studies have shown its role in promoting colon,<sup>3</sup> breast,<sup>4</sup> and prostate<sup>5</sup> cancers. This makes it an attractive target for therapy. For example, a cholesterol synthesis inhibitor can induce apoptosis in prostate cancer cells<sup>6</sup> by targeting their elevated cholesterol synthesis.<sup>7</sup> Additionally,  $M\beta CD$ , a millimolar cholesterol-depleting agent, augments the efficacy of tamoxifen in breast cancer<sup>8</sup> and melanoma cells<sup>9</sup> due to higher expression of cholesterol-rich microdomains in tumor cells.<sup>10,11</sup> Cheng et al. reported the link between intracellular cholesterol accumulation and enhanced cancer aggressiveness.<sup>12</sup> Depleting cholesteryl ester storage by blocking cholesterol esterification is being explored in various cancers.<sup>12–15</sup> We recently used peptides to conjugate with cholesterol/lipids.<sup>16,17</sup> The conjugates act as a substrate of enzymatic noncovalent synthesis<sup>18</sup> for killing drug-resistant cancer cells through in situ self-assembly.<sup>16,17</sup> These studies altogether open up the possibility of applying peptide assemblies to target cholesterol and lipid metabolism for developing cancer therapeutics.

During our studies of unnatural peptide assemblies, we coincidentally found that the peptide assemblies deplete cholesterol and inhibit cancer cells. The peptide bb-NBD (**1**), containing D-BiP (or b) and C-terminal capped by a fluorophore (NBD), self-assembles to form micelles. **1** enters cells rapidly, and  $M\beta CD$  enhances cellular uptake of **1**. Click reaction<sup>19</sup> reveals that **1** depletes cholesterol from the cell membrane (Scheme 1). Fluorescent imaging indicates that **1** distributes in membrane-rich organelles, such as the ER, Golgi apparatus, and lysosomes. More importantly, **1** potently inhibits malignant cancer cells (e.g., HeLa and PC3), exhibiting synergism with either an acute or a chronic

cholesterol lowering agent. We also found that C-terminal capping and unnatural amino acid residues (i.e., BiP) are necessary for the observed cholesterol depletion and potent cancer cell inhibition. This work suggests that engineering of unnatural peptide assemblies is a useful methodology to develop a molecular platform that targets the cell membrane for treating diseases, including cancer.

To enhance the efficacy of peptides for self-assembly, we replaced the D-phenylalanine with an unnatural amino acid, D-BiP because it possesses enhanced hydrophobicity and biphenyl motif appears to favor cellular uptake.<sup>20–22</sup> This rationale leads to a less explored<sup>23,24</sup> self-assembling motif, D-BiP-D-BiP or bb. To visualize the peptide assemblies in live cells, we added NBD, a fluorophore, to the C-terminus of bb. This design creates an unnatural peptide, bb-NBD or **1** (Scheme 1). Additionally, we designed two analogs, NBD-bb (**2**) and ff-NBD (**3**), as the controls of **1** for examining the roles of the position of the fluorophore and the self-assembling motif, respectively.

SPPS and RP-HPLC yielded purified peptides. CMC values for **1**, **2**, and **3** are 14.8, 373, and 20.6  $\mu M$  (Figures S3–S5), respectively. **1**'s lower CMC compared to **2** aligns with protein N-/C-termini  $pK_a$  (7.7/3.3).<sup>25</sup> TEM revealed nanospheres formed by **1** above CMC (with an average hydrodynamic radius of  $103.2 \pm 1.9$  nm measured by DLS) and is hardly visible below CMC (Figures S6 and S7). In contrast, **2** and **3** only form amorphous aggregates above and below their CMCs

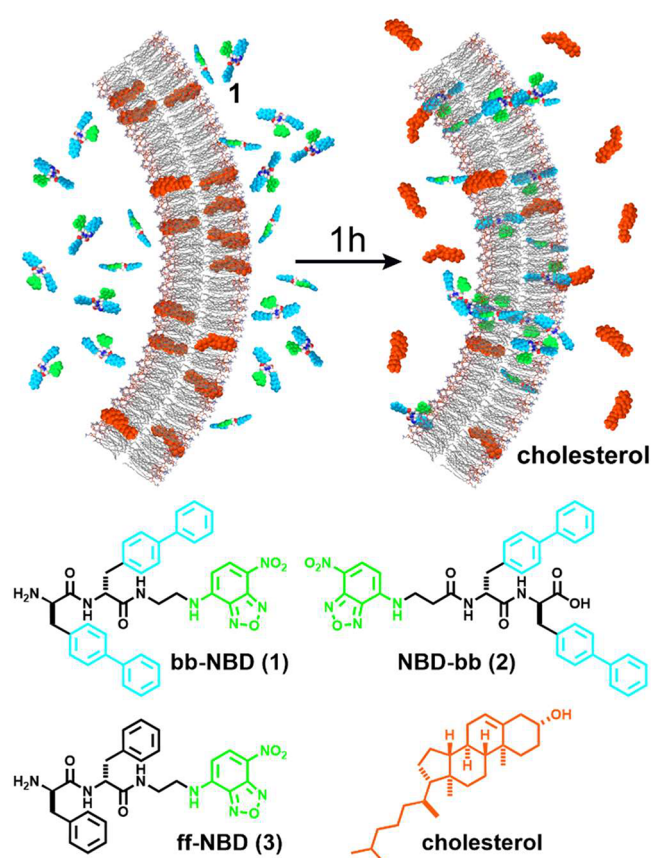
Received: March 1, 2024

Revised: April 29, 2024

Accepted: April 30, 2024

Published: May 3, 2024



Scheme 1. Rapid Cholesterol Depletion from Membranes by **1** and the Structures of **1** and Its Analogs

(Figures S8 and S9). These results indicate that a bb motif and an exposed amine group are crucial for **1**'s self-assembly in water.

We used CLSM to visualize the cellular uptake of assemblies of **1** in HeLa cells (Figure 1). The rapid cellular uptake of **1** is

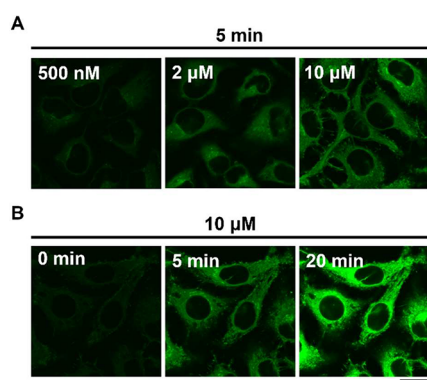


**Figure 1.** Confocal microscopy: HeLa cells treated with **1** (A, dose response; B, 10  $\mu$ M time-lapse) (Bar = 20  $\mu$ m).

both concentration- and time-dependent (Figures 1A, 1B and S10). For instance, 500 nM of **1** shows noticeable internalization in merely 5 min (Figure 1A), while 10  $\mu$ M of **1** gets significantly enriched intracellularly in 20 min (Figure 1B). These results suggest that monomers of **1** (below CMC) insert into the cell membrane rapidly, and **1** (at about CMC) likely

forms assemblies inside the cell membrane to exhibit brighter fluorescence.

We then used endocytosis inhibitors<sup>26</sup> to provide more insights into the quick internalization of **1**. Dynasore blocks the uptake of **1** (Figures 2A and S11), suggesting **1** enters cells through an energy-requiring process. In addition, other inhibitors, for example, CPZ and Retro-2 also partially reduce the uptake of **1** (Figures 2A and S11), indicating a hybrid mode of endocytosis. However, M $\beta$ CD, a common inhibitor of cholesterol-dependent endocytosis, unexpectedly enhances the uptake of **1** significantly (Figures 2A, S11 and S12). The intracellular fluorescence intensity of **1** in the M $\beta$ CD treated group is over two times higher than that of the control group in 10 min (Figure 2B). Single-cell analysis confirms that increasing M $\beta$ CD concentration boosts the uptake of **1** (Figures 2C and S13). For example, 1 mM M $\beta$ CD increases **1**'s uptake by 1.6-fold in 10 min, while 5 mM M $\beta$ CD increases it by 2.2-fold (Figure 2D). Since M $\beta$ CD removes cellular cholesterol,<sup>27</sup> we believe that **1** enters cells to fill these vacancies (Figures 2C and S13).

M $\beta$ CD also influences the translocation of **1**, evidenced by more green fluorescence on the membrane region compared to the group without M $\beta$ CD (Figure S13). We stained the cells with a PM dye, CPDR, to better visualize the distribution of **1** under cholesterol depletion conditions and verify the translocation. The fluorescence of CPDR is much weaker in the M $\beta$ CD treated group compared to the control group, implying the successful depletion of cholesterol (Figures S14 and S15). After the addition of **1**, strong green fluorescence appears instantaneously at the PM region, with a good colocalization with CPDR (Figures 2E and S16). In contrast, **1** mainly localizes in the intracellular region in the control group, with a poor colocalization with PM (Figures 2E and S16). Furthermore, quantifying green fluorescence on the PM region shows that 60% of **1** presents on PM in the M $\beta$ CD treated group immediately after the addition of **1**, in comparison to 33% in the control group (Figure S17). Although **1** distributes from membrane to cytoplasm over time in both groups, the M $\beta$ CD treated group retains significantly more **1** on PM—about 45% (Figure S17). Since the PM is rich in cellular cholesterol,<sup>28</sup> these results suggest that after M $\beta$ CD acutely depletes cholesterol, **1** preferentially assembles at former cholesterol-rich membrane regions. This implies that **1** has a high affinity for cholesterol insertion sites under depletion conditions.

Knowing that **1** exhibits strong affinity for cholesterol-rich membranes, particularly when cholesterol is depleted by M $\beta$ CD, we employed the bioorthogonal CuAAC click reaction<sup>19</sup> to examine the potential competition between **1** and cholesterol itself. After M $\beta$ CD depleted endogenous cholesterol, cells were coincubated with **1** and chol-azide (as a membrane insertion competitor, Scheme S4). CLSM after click reaction with Cy5 alkyne showed minimal Cy5 fluorescence in coincubated cells (**1** + chol-azide) compared to the strong signal with chol-azide alone (Figure S18). This suggests that **1** preferentially binds to vacated cholesterol sites upon depletion.

We tested if **1** displaces cholesterol without M $\beta$ CD. Cells pretreated with chol-azide were incubated with **1**, and then visualized. CLSM confirmed that **1** reduces cholesterol (Figures 2F, S19 and S20). Remarkably, **1** induces a 74% and 88% cholesterol depletion within 1 h and 2 h, respectively (Figure 2G). While depletion remained significant up to 8 h, it reached 40% after 24 h due to intracellular aggregation of **1**

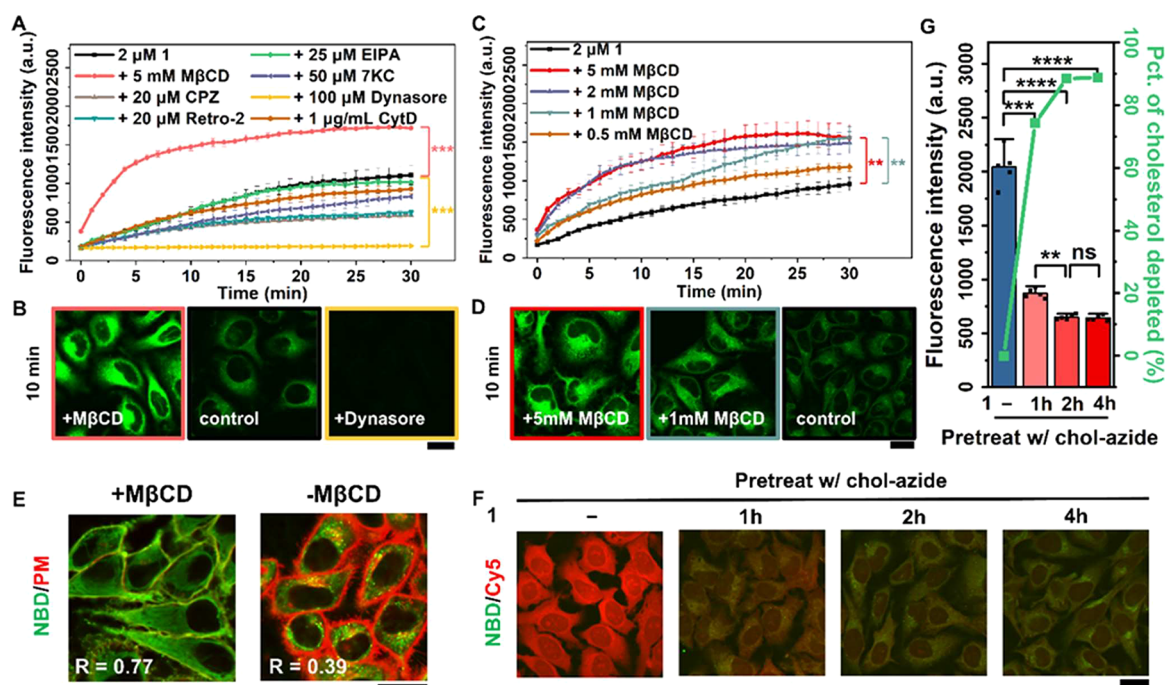


**Figure 2.** HeLa cells treated with  $2 \mu\text{M}$  **1**: (A) Endocytosis inhibitor effects (quantification). (B, D) Images with  $\text{M}\beta\text{CD}$ /Dynasore pretreatment (CLSM). (C)  $\text{M}\beta\text{CD}$  dose dependence (quantification). (E) Instantaneous treatment with/without  $\text{M}\beta\text{CD}$  (CLSM with CellMask stain). (F, G) Cholesterol depletion with pretreatment (CLSM and quantification) (Scale bar =  $20 \mu\text{m}$ ).

(Figure S21). In contrast, a parallel experiment where cells were pretreated with **1** demonstrated that the subsequent addition of chol-azide was unable to displace **1** from the cell membranes (Figure S22). These findings suggest that **1** not only has a stronger affinity to vacant cholesterol insertion sites than cholesterol itself but also can directly insert into membranes and replace cholesterol, demonstrating the unique cholesterol depletion action of **1**. Furthermore, we tested whether  $\text{M}\beta\text{CD}$  could remove **1** from cell membranes as it does with cholesterol. After pretreating HeLa cells with **1** for 1 h, we added  $\text{M}\beta\text{CD}$  to the cells for another 30 min. Compared to cells treated with only **1** for 1.5 h,  $\text{M}\beta\text{CD}$  treated cells show no significant changes in the fluorescence intensity of **1**, further confirming the strong affinity of **1** to cell membranes (Figure S23). However, immunostaining of LDLR, which mediates the endocytosis of cholesterol, shows an inverse relationship between **1** and LDLR, indicating LDLR-independent internalization of **1** (Figure S24).

To better understand the intracellular distribution of **1**, we used various trackers or transfection methods to stain different organelles in HeLa cells. This was done to analyze colocalization with **1** using CLSM (Figure S25). When the cells were treated with **1** for 20 min, we observed significant overlaps of its green fluorescence with ER, Golgi apparatus, and lysosomes. This was evidenced by high M2 values (fraction of organelle overlapping **1**) of over 0.9 (Figures 3A, C and S26). Time-lapse CLSM images demonstrate the rapid targeting of these organelles by **1**, with noticeable colocalization within 5 min and pronounced enrichment at ER within 10 min (Figures 3B and S27). Given that these membrane-bound organelles are crucial for cholesterol transport and biosynthesis,<sup>29</sup> our findings imply that **1** has a strong affinity for intracellular cholesterol-rich membranes, in addition to the PM.

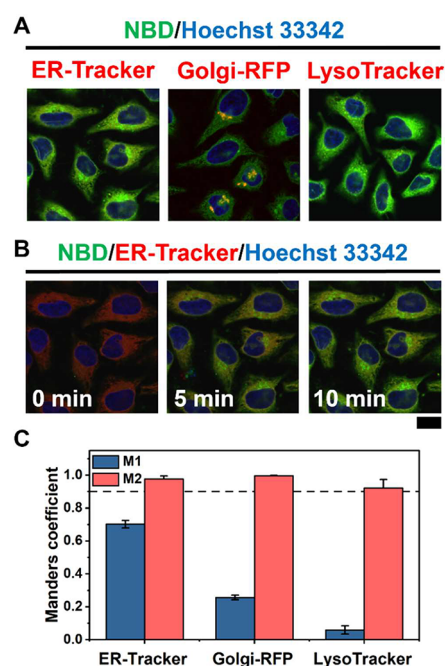


**Figure 3.** (A) HeLa cells stained with trackers, treated with **1** ( $2 \mu\text{M}$ , 20 min), and imaged (CLSM). (B) Time-lapse of ER-stained cells treated with **1** ( $2 \mu\text{M}$ , CLSM). (C) Colocalization analysis (Manders' coefficients) of **1** vs trackers (Scale bar =  $20 \mu\text{m}$ ).

Based on the unique cholesterol depletion behavior of **1**, we tested its cytotoxicity against HeLa and PC3 cells. MTT assay revealed that **1** exhibits strong cytotoxicity against both cell lines, with  $\text{IC}_{50}$  values of 10.3 and  $13.7 \mu\text{M}$ , respectively (Figures 4A–C and S28–29). Furthermore, the cytotoxicity of compound **1** increases with time (Figure 4C), suggesting that it inhibits cancer cells related to its intracellular accumulation.

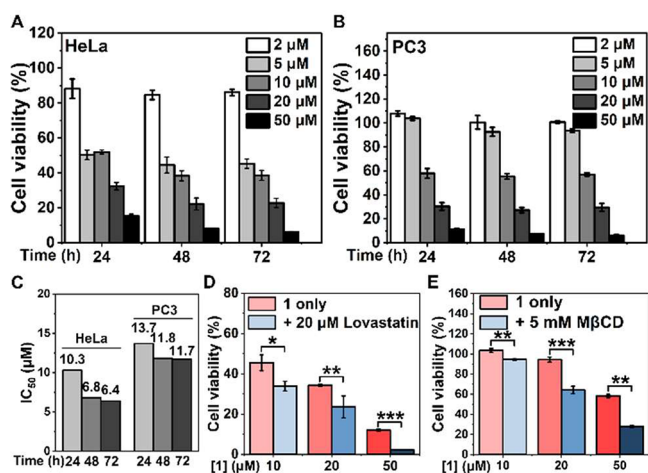


**Figure 4.** Cell viability of (A) HeLa and (B) PC3 cells treated with **1** and (C) the  $IC_{50}$  values of **1** against HeLa and PC3 cells. Cell viability of HeLa cells treated (D) with **1** (24 h), with or without the addition of Lovastatin (20  $\mu$ M) and (E) with **1** (1 h), with or without M $\beta$ CD (5 mM, 30 min) pretreatment.

Moreover, **1** exhibits synergism with other cholesterol depletion agents. Co-incubating **1** with lovastatin and M $\beta$ CD, which deplete cholesterol by inhibiting cholesterol biosynthesis<sup>30</sup> and cholesterol extraction,<sup>27</sup> respectively, significantly decreases cell viability in a concentration-dependent manner (Figures 4D,E and S30–36). Given the enhanced cellular uptake under cholesterol depletion conditions, these results suggest that the cytotoxicity induced by **1** is positively correlated with its intracellular accumulation.

To elucidate the cell death pathways triggered by **1**, we employed a series of cell death inhibitors. Our results indicate **1** induces cell death through multiple pathways, including apoptosis, necrosis, and oncosis (Figures S37–39). Further investigation using lysosomal staining reveals that **1** induces an enlargement of lysosomes (Figure S40). Additionally, immunostaining demonstrated a concentration-dependent increase in LC3B expression (Figure S41). Western blot analysis of LC3 also clearly reveals its upregulation induced by **1** (Figure S42). These combined observations suggest autophagic cell death.

We compared compounds (**1**, **2**, and **3**) for their cholesterol depletion in HeLa cells. CLSM shows that **2**, possessing a carboxylate C-terminus, localizes to the PM exterior (Figure S43), supporting the bb motif's membrane targeting. Unlike **1**, **2**'s poor uptake (likely due to its C-terminal negative charges) results in low cytotoxicity ( $IC_{50} > 200 \mu$ M, Figure S44). Conversely, **3**, with an ff motif, shows rapid uptake (Figure S45), suggesting a diffusion mechanism different from **1** (Figure S46). Inhibitor studies further confirm this (Figures S47–S48): neither M $\beta$ CD nor dynasore significantly affects **3**'s uptake. Although M $\beta$ CD boosts the uptake of **1** by more than 2-fold in 5 min, it has a minimal impact on **3**, confirming the bb motif's exclusive cholesterol depletion function (Figure S49). Despite fast uptake, **3** exhibits mild cytotoxicity against HeLa cells due to its lack of cholesterol targeting (Figure S50).

In conclusion, we demonstrated a novel, unnatural peptide assembly with remarkable abilities: rapid cholesterol depletion in cancer cells and potent cytotoxicity against malignant cancer cells. The amine group of **1** likely contributes to displace cholesterol due to the stronger lipid head affinity. Crucially,

this work highlights the versatility of peptide assemblies<sup>31–43</sup> in targeting cholesterol-rich membranes and hindering cancer cell proliferation. **1** showed selectivity for HeLa cells over PC3 and HepG2 (Figure S51), which correlates with higher LDLR expression in PC3 and HepG2.<sup>44</sup> Lovastatin treatment further enhanced **1**'s selectivity for PC3 over HepG2 cells (Figure S52). This approach paves the way for further therapeutic development by integrating unnatural amino acids with distinct cancer-targeting mechanisms, such as redox reactions<sup>45–47</sup> or enzymatic processes,<sup>48–54</sup> to target cell membrane<sup>55</sup> and modulate aberrant lipid metabolism in cells.

## ■ ASSOCIATED CONTENT

### Supporting Information

The Supporting Information is available free of charge at <https://pubs.acs.org/doi/10.1021/jacs.4c03101>.

Materials and detailed experimental procedures, TEM and CLSM images, cells viabilities, LC/MS spectra, chemical structures of the compounds (PDF)

**Movie 1:** **1** (2  $\mu$ M) incubated with HeLa cells over 30 min (AVI)

**Movie 2:** **1** (2  $\mu$ M) and M $\beta$ CD (5 mM) incubated with HeLa cells over 30 min (AVI)

**Movie 3:** **1** (2  $\mu$ M) incubated with HeLa cells over 5 min (AVI)

**Movie 4:** **1** (2  $\mu$ M) and M $\beta$ CD (5 mM) incubated with HeLa cells over 5 min (AVI)

## ■ AUTHOR INFORMATION

### Corresponding Author

Bing Xu – Department of Chemistry, Brandeis University, Waltham, Massachusetts 02453, United States; [orcid.org/0000-0002-4639-387X](https://orcid.org/0000-0002-4639-387X); Email: [bxu@brandeis.edu](mailto:bxu@brandeis.edu)

### Authors

Qiuxin Zhang – Department of Chemistry, Brandeis University, Waltham, Massachusetts 02453, United States; [orcid.org/0000-0002-8659-3569](https://orcid.org/0000-0002-8659-3569)

Weiyi Tan – Department of Chemistry, Brandeis University, Waltham, Massachusetts 02453, United States; [orcid.org/0000-0001-5316-8278](https://orcid.org/0000-0001-5316-8278)

Zhiyu Liu – Department of Chemistry, Brandeis University, Waltham, Massachusetts 02453, United States

Yichi Zhang – Department of Chemistry, Brandeis University, Waltham, Massachusetts 02453, United States

Wei-Shao Wei – Martin A. Fisher School of Physics, Brandeis University, Waltham, Massachusetts 02453, United States

Seth Fraden – Martin A. Fisher School of Physics, Brandeis University, Waltham, Massachusetts 02453, United States

Complete contact information is available at:

<https://pubs.acs.org/doi/10.1021/jacs.4c03101>

### Notes

The authors declare no competing financial interest.

## ■ ACKNOWLEDGMENTS

This work was partially supported by NIH grants CA142746, CA252364, and the NSF DMR-2011846 MRSEC program at Brandeis, including its Light Scattering Facility. We also acknowledge a NIH Shared Instrumentation grant (1S10OD034395).

## ■ ABBREVIATIONS

CPDR, CellMask PM Deep Red; chol-azide, cholesteryl-TEG-azide; CLSM, confocal laser scanning microscopy; CMC, critical micelle concentrations; CPZ, chlorpromazine; D-BiP or b, D-4,4'-biphenylalanine; DLS, dynamic light scattering; ER, endoplasmic reticulum; LDLR, low density lipoprotein receptor; M $\beta$ CD, methyl- $\beta$ -cyclodextrin; NBD, nitrobenzoxadiazole; LC3B, Microtubule-associated protein 1 light chain 3 beta; PM, plasma membrane; RP-HPLC, reverse phase high performance liquid chromatography; SPPS, solid-phase peptide synthesis; TEM, transmission electron microscopy

## ■ REFERENCES

- (1) Haslam, D. W.; James, W. P. T. Obesity. *Lancet* **2005**, *366* (9492), 1197–1209.
- (2) Silvente-Poirot, S.; Poirot, M. Cholesterol metabolism and cancer: the good, the bad and the ugly. *Curr. Opin. Pharm.* **2012**, *12* (6), 673–676.
- (3) Degirolamo, C.; Modica, S.; Palasciano, G.; Moschetta, A. Bile acids and colon cancer: Solving the puzzle with nuclear receptors. *Trends Mol. Med.* **2011**, *17* (10), 564–572.
- (4) Finlay-Schultz, J.; Sartorius, C. A. Steroid Hormones, Steroid Receptors, and Breast Cancer Stem Cells. *J. Mammary Gland Biol. Neoplasia* **2015**, *20* (1), 39–50.
- (5) Bader, D. A.; McGuire, S. E. Tumour metabolism and its unique properties in prostate adenocarcinoma. *Nat. Rev. Urology* **2020**, *17* (4), 214–231.
- (6) Zhuang, L.; Kim, J.; Adam, R. M.; Solomon, K. R.; Freeman, M. R. Cholesterol targeting alters lipid raft composition and cell survival in prostate cancer cells and xenografts. *J. Clin. Invest.* **2005**, *115* (4), 959–968.
- (7) Mo, H.; Elson, C. E. Studies of the isoprenoid-mediated inhibition of mevalonate synthesis applied to cancer chemotherapy and chemoprevention. *Exp. Biol. Med.* **2004**, *229* (7), 567–585.
- (8) Tiwary, R.; Yu, W.; Degraffenried, L. A.; Sanders, B. G.; Kline, K. Targeting cholesterol-rich microdomains to circumvent tamoxifen-resistant breast cancer. *Breast Cancer Res.* **2011**, *13*, 1–12.
- (9) Mohammad, N.; Malvi, P.; Meena, A. S.; Singh, S. V.; Chaube, B.; Vannuruswamy, G.; Kulkarni, M. J.; Bhat, M. K. Cholesterol depletion by methyl- $\beta$ -cyclodextrin augments tamoxifen induced cell death by enhancing its uptake in melanoma. *Mol. Cancer* **2014**, *13* (1), 1–13.
- (10) Li, Y. C.; Park, M. J.; Ye, S.-K.; Kim, C.-W.; Kim, Y.-N. Elevated levels of cholesterol-rich lipid rafts in cancer cells are correlated with apoptosis sensitivity induced by cholesterol-depleting agents. *Am. J. Pathol.* **2006**, *168* (4), 1107–1118.
- (11) Patra, S. K. Dissecting lipid raft facilitated cell signaling pathways in cancer. *BBA-Rev. Cancer* **2008**, *1785* (2), 182–206.
- (12) Yue, S.; Li, J.; Lee, S.-Y.; Lee, H. J.; Shao, T.; Song, B.; Cheng, L.; Masterson, T. A.; Liu, X.; Ratliff, T. L.; Cheng, J.-X. Cholesteryl ester accumulation induced by PTEN loss and PI3K/AKT activation underlies human prostate cancer aggressiveness. *Cell Metab.* **2014**, *19* (3), 393–406.
- (13) Lee, S. S.-Y.; Li, J.; Tai, J. N.; Ratliff, T. L.; Park, K.; Cheng, J.-X. Avasimibe encapsulated in human serum albumin blocks cholesterol esterification for selective cancer treatment. *ACS Nano* **2015**, *9* (3), 2420–2432.
- (14) Li, J.; Gu, D.; Lee, S. S.; Song, B.; Bandyopadhyay, S.; Chen, S.; Konieczny, S. F.; Ratliff, T. L.; Liu, X.; Xie, J.; Cheng, J.-X. Abrogating cholesterol esterification suppresses growth and metastasis of pancreatic cancer. *Oncogene* **2016**, *35* (50), 6378–6388.
- (15) Lee, H. J.; Li, J.; Vickman, R. E.; Li, J.; Liu, R.; Durkes, A. C.; Elzey, B. D.; Yue, S.; Liu, X.; Ratliff, T. L.; Cheng, J.-X. Cholesterol esterification inhibition suppresses prostate cancer metastasis by impairing the Wnt/ $\beta$ -catenin pathway. *Mol. Cancer Res.* **2018**, *16* (6), 974–985.
- (16) Wang, H.; Feng, Z.; Wu, D.; Fritzsching, K. J.; Rigney, M.; Zhou, J.; Jiang, Y.; Schmidt-Rohr, K.; Xu, B. Enzyme-regulated supramolecular assemblies of cholesterol conjugates against drug-resistant ovarian cancer cells. *J. Am. Chem. Soc.* **2016**, *138* (34), 10758–10761.
- (17) Wang, J.; Tan, W.; Li, G.; Wu, D.; He, H.; Xu, J.; Yi, M.; Zhang, Y.; Aghvami, S. A.; Fraden, S.; Xu, B. Enzymatic insertion of lipids increases membrane tension for inhibiting drug resistant cancer cells. *Chem.—Eur. J.* **2020**, *26* (66), 15116–15120.
- (18) He, H.; Tan, W.; Guo, J.; Yi, M.; Shy, A. N.; Xu, B. Enzymatic Noncovalent Synthesis. *Chem. Rev.* **2020**, *120* (18), 9994–10078.
- (19) Kolb, H. C.; Finn, M.; Sharpless, K. B. Click chemistry: diverse chemical function from a few good reactions. *Angew. Chem., Int. Ed.* **2001**, *40* (11), 2004–2021.
- (20) Yi, M.; Wang, F.; Tan, W.; Hsieh, J. T.; Egelman, E. H.; Xu, B. Enzyme Responsive Rigid-Rod Aromatics Target “Undruggable” Phosphatases to Kill Cancer Cells in a Mimetic Bone Microenvironment. *J. Am. Chem. Soc.* **2022**, *144* (29), 13055–13059.
- (21) Guo, J.; Tan, W.; He, H.; Xu, B. Autohydrolysis of Diglycine-Activated Succinic Esters Boosts Cellular Uptake. *Angew. Chem., Int. Ed.* **2023**, *62* (36), No. e202308022.
- (22) Li, F.; Li, Y.; Zhou, Z.; Lv, S.; Deng, Q.; Xu, X.; Yin, L. Engineering the Aromaticity of Cationic Helical Polypeptides toward “self-Activated” DNA/siRNA Delivery. *ACS Appl. Mater. Interfaces* **2017**, *9* (28), 23586–23601.
- (23) Reches, M.; Gazit, E. Designed aromatic homo-dipeptides: formation of ordered nanostructures and potential nanotechnological applications. *Phys. Biol.* **2006**, *3* (1), S10.
- (24) Ochi, R.; Nishida, T.; Ikeda, M.; Hamachi, I. Design of peptide-based bolaamphiphiles exhibiting heat-set hydrogelation via retro-Diels-Alder reaction. *J. Mater. Chem. B* **2014**, *2* (11), 1464–1469.
- (25) Grimsley, G. R.; Scholtz, J. M.; Pace, C. N. A summary of the measured pK values of the ionizable groups in folded proteins. *Protein Sci.* **2009**, *18* (1), 247–251.
- (26) Sousa de Almeida, M.; Susnik, E.; Drasler, B.; Taladriz-Blanco, P.; Petri-Fink, A.; Rothen-Rutishauser, B. Understanding nanoparticle endocytosis to improve targeting strategies in nanomedicine. *Chem. Soc. Rev.* **2021**, *50* (9), 5397–5434.
- (27) Zidovetzki, R.; Levitan, I. Use of cyclodextrins to manipulate plasma membrane cholesterol content: evidence, misconceptions and control strategies. *BBA-Biomembranes* **2007**, *1768* (6), 1311–1324.
- (28) Chu, B.-B.; Liao, Y.-C.; Qi, W.; Xie, C.; Du, X.; Wang, J.; Yang, H.; Miao, H.-H.; Li, B.-L.; Song, B.-L. Cholesterol transport through lysosome-peroxisome membrane contacts. *Cell* **2015**, *161* (2), 291–306.
- (29) Ikonen, E.; Zhou, X. Cholesterol transport between cellular membranes: A balancing act between interconnected lipid fluxes. *Developmental Cell* **2021**, *56* (10), 1430–1436.
- (30) Clendening, J.; Penn, L. Targeting tumor cell metabolism with statins. *Oncogene* **2012**, *31* (48), 4967–4978.
- (31) Jiang, T.; Xu, C.; Liu, Y.; Liu, Z.; Wall, J. S.; Zuo, X.; Lian, T.; Salaita, K.; Ni, C.; Pochan, D.; Conticello, V. P. Structurally defined nanoscale sheets from self-assembly of collagen-mimetic peptides. *J. Am. Chem. Soc.* **2014**, *136* (11), 4300–4308.
- (32) Nagy, K. J.; Giano, M. C.; Jin, A.; Pochan, D. J.; Schneider, J. P. Enhanced mechanical rigidity of hydrogels formed from enantiomeric peptide assemblies. *J. Am. Chem. Soc.* **2011**, *133* (38), 14975–14977.
- (33) Wang, H.; Song, Y.; Wang, W.; Chen, N.; Hu, B.; Liu, X.; Zhang, Z.; Yu, Z. Organelle-Mediated Dissipative Self-Assembly of Peptides in Living Cells. *J. Am. Chem. Soc.* **2024**, *146* (1), 330–341.
- (34) Liu, X.; Li, M.; Liu, J.; Song, Y.; Hu, B.; Wu, C.; Liu, A.-A.; Zhou, H.; Long, J.; Shi, L.; Yu, Z. In situ self-sorting peptide assemblies in living cells for simultaneous organelle targeting. *J. Am. Chem. Soc.* **2022**, *144* (21), 9312–9323.
- (35) Shi, J.; Fichman, G.; Schneider, J. P. Enzymatic Control of the Conformational Landscape of Self-Assembling Peptides. *Angew. Chem., Int. Ed.* **2018**, *57* (35), 11188–11192.
- (36) Yu, Z.; Erbas, A.; Tantakitti, F.; Palmer, L. C.; Jackman, J. A.; Olvera de la Cruz, M.; Cho, N.-J.; Stupp, S. I. Co-assembly of peptide

- amphiphiles and lipids into supramolecular nanostructures driven by anion- $\pi$  interactions. *J. Am. Chem. Soc.* **2017**, *139* (23), 7823–7830.
- (37) Su, H.; Zhang, W.; Wang, H.; Wang, F.; Cui, H. Paclitaxel-promoted supramolecular polymerization of peptide conjugates. *J. Am. Chem. Soc.* **2019**, *141* (30), 11997–12004.
- (38) Magnotti, E. L.; Hughes, S. A.; Dillard, R. S.; Wang, S.; Hough, L.; Karumbakandathil, A.; Lian, T.; Wall, J. S.; Zuo, X.; Wright, E. R.; Conticello, V. P. Self-assembly of an  $\alpha$ -helical peptide into a crystalline two-dimensional nanoporous framework. *J. Am. Chem. Soc.* **2016**, *138* (50), 16274–16282.
- (39) König, N.; Szostak, S. M.; Nielsen, J. E.; Dunbar, M.; Yang, S.; Chen, W.; Benjamin, A.; Radulescu, A.; Mahmoudi, N.; Willner, L.; Ketten, S.; Dong, H.; Lund, R. Stability of nanopeptides: structure and molecular exchange of self-assembled peptide fibers. *ACS Nano* **2023**, *17* (13), 12394–12408.
- (40) Yang, L.; Peltier, R.; Zhang, M.; Song, D.; Huang, H.; Chen, G.; Chen, Y.; Zhou, F.; Hao, Q.; Bian, L.; He, M. L.; Wang, Z.; Hu, Y.; Sun, H. Desuccinylation-triggered peptide self-assembly: live cell imaging of SIRT5 activity and mitochondrial activity modulation. *J. Am. Chem. Soc.* **2020**, *142* (42), 18150–18159.
- (41) Yu, S.; Xian, S.; Ye, Z.; Pramudya, I.; Webber, M. J. Glucose-Fueled Peptide Assembly: Glucagon Delivery via Enzymatic Actuation. *J. Am. Chem. Soc.* **2021**, *143* (32), 12578–12589.
- (42) Silva, G. A.; Czeisler, C.; Niece, K. L.; Beniash, E.; Harrington, D. A.; Kessler, J. A.; Stupp, S. I. Selective differentiation of neural progenitor cells by high-epitope density nanofibers. *Science* **2004**, *303* (5662), 1352–5.
- (43) Berndt, P.; Fields, G. B.; Tirrell, M. Synthetic lipidation of peptides and amino acids: monolayer structure and properties. *J. Am. Chem. Soc.* **1995**, *117* (37), 9515–9522.
- (44) Uhlen, M.; Zhang, C.; Lee, S.; Sjöstedt, E.; Fagerberg, L.; Bidkhor, G.; Benfeitas, R.; Arif, M.; Liu, Z.; Edfors, F.; Sanli, K.; von Feilitzen, K.; Oksvold, P.; Lundberg, E.; Hober, S.; Nilsson, P.; Mattsson, J.; Schwenk, J. M.; Brunnström, H.; Glimelius, B.; Sjöblom, T.; Edqvist, P.-H.; Djureinovic, D.; Micke, P.; Lindskog, C.; Mardinoglu, A.; Ponten, F. A pathology atlas of the human cancer transcriptome. *Science* **2017**, *357* (6352), No. eaan2507.
- (45) Zhan, J.; Cai, Y.; He, S.; Wang, L.; Yang, Z. Tandem molecular self-assembly in liver cancer cells. *Angew. Chem., Int. Ed.* **2018**, *57* (7), 1813–1816.
- (46) Shi, Y.; Wang, J.; Wang, H.; Hu, Y.; Chen, X.; Yang, Z. Glutathione-triggered formation of a Fmoc-protected short peptide-based supramolecular hydrogel. *PLoS One* **2014**, *9* (9), No. e106968.
- (47) Ye, D.; Pandit, P.; Kempen, P.; Lin, J.; Xiong, L.; Sinclair, R.; Rutt, B.; Rao, J. Redox-triggered self-assembly of gadolinium-based MRI probes for sensing reducing environment. *Bioconjugate Chem.* **2014**, *25* (8), 1526–1536.
- (48) Liu, X.; Zhan, W.; Gao, G.; Jiang, Q.; Zhang, X.; Zhang, H.; Sun, X.; Han, W.; Wu, F.-G.; Liang, G. Apoptosis-Amplified Assembly of Porphyrin Nanofiber Enhances Photodynamic Therapy of Oral Tumor. *J. Am. Chem. Soc.* **2023**, *145* (14), 7918–7930.
- (49) Ye, D.; Shuhendler, A. J.; Cui, L.; Tong, L.; Tee, S. S.; Tikhomirov, G.; Felsner, D. W.; Rao, J. Bioorthogonal cyclization-mediated in situ self-assembly of small-molecule probes for imaging caspase activity in vivo. *Nat. Chem.* **2014**, *6* (6), 519–526.
- (50) Tang, W.; Zhao, Z.; Chong, Y.; Wu, C.; Liu, Q.; Yang, J.; Zhou, R.; Lian, Z.-X.; Liang, G. Tandem enzymatic self-assembly and slow release of dexamethasone enhances its antihepatic fibrosis effect. *ACS Nano* **2018**, *12* (10), 9966–9973.
- (51) Hai, Z.; Li, J.; Wu, J.; Xu, J.; Liang, G. Alkaline phosphatase-triggered simultaneous hydrogelation and chemiluminescence. *J. Am. Chem. Soc.* **2017**, *139* (3), 1041–1044.
- (52) Tanaka, A.; Fukuoka, Y.; Morimoto, Y.; Honjo, T.; Koda, D.; Goto, M.; Maruyama, T. Cancer cell death induced by the intracellular self-assembly of an enzyme-responsive supramolecular gelator. *J. Am. Chem. Soc.* **2015**, *137* (2), 770–775.
- (53) Hughes, M.; Debnath, S.; Knapp, C. W.; Ulijn, R. V. Antimicrobial properties of enzymatically triggered self-assembling aromatic peptide amphiphiles. *Biomater. Sci.* **2013**, *1* (11), 1138–1142.
- (54) Marciano, Y.; Del Solar, V.; Nayeem, N.; Dave, D.; Son, J.; Contel, M.; Ulijn, R. V. Encapsulation of Gold-Based Anticancer Agents in Protease-Degradable Peptide Nanofilaments Enhances Their Potency. *J. Am. Chem. Soc.* **2023**, *145* (1), 234–246.
- (55) Wu, X.; Hu, J. J.; Yoon, J. Cell Membrane as A Promising Therapeutic Target: From Materials Design to Biomedical Applications. *Angew. Chem., Int. Ed.* **2024**, *136*, No. e202400249.